Check for updates

Phase textures of metal–oxide nanocomposites self-orchestrated by atomic diffusions through precursor alloys†

Nasrat Hannah Shudin,[ab] Ryuto Eguchi,[ac] Takeshi Fujita, [ID] *[d] Tomoharu Tokunaga,[e] Ayako Hashimoto [ID] [ac] and Hideki Abe [ID] *[ab]

Metal-oxide nanocomposites (MONs) are of pivotal importance as electrode materials, yet lack a guiding principle to tune their phase texture. Here we report that the phase texture of MONs can be tuned at the nanoscale by controlling the nanophase separation of precursor alloys. *In situ* transmission electron microscopy (*in situ* TEM) has demonstrated that a MON material of platinum (Pt) and cerium oxide (CeO_2) is obtained through promoted nanophase separation of a Pt_5Ce precursor alloy in an atmosphere containing oxygen (O_2) and carbon monoxide (CO). The Pt–CeO_2 MON material comprised an alternating stack of nanometre-thick layers of Pt and CeO_2 in different phase textures ranging from lamellae to mazes, depending on the O_2 fraction in the atmosphere. Mathematical simulations have demonstrated that the phase texture of MONs originates from a balance in the atomic diffusions across the alloy precursor, which is controllable by the O_2 fraction, temperature, and composition of the precursor alloys.

1. Introduction

Metal-oxide nanocomposites (MONs) are of confocal interest in industries and day-to-day life due to their prominent functionalities as electrodes of batteries and/or fuel cells.[1–3] MONs are usually materialized by assembling nano-scale building blocks of metal and oxides through bottom-up approaches including mechanical mixing, sol–gel processes, or coprecipitation methods.[4–10] Indeed, nano-scale particles of nickel (Ni) and yttria-stabilized zirconia

[a] National Institute for Materials Science, Namiki 1-1, Tsukuba, Ibaraki 305-00443, Japan. E-mail: ABE.Hideki@nims.go.jp

[b] Graduate School of Science and Engineering, Saitama University, Shimo-Okubo 255, Saitama 338-8570, Japan

[c] Tsukuba University, 1-chome-1-1 Tennodai, Tsukuba, Ibaraki 305-8577, Japan

[d] Kohchi University of Technology, Kami, Kochi, Japan

[e] Institute of Materials and Systems for Sustainability, Nagoya University, Furo-cho, Chikusa-ku, Nagoya 464-8601, Japan

† Electronic supplementary information (ESI) available. See DOI: https://doi.org/10.1039/d3cp05157a

(YSZ) materials are mixed with high-speed ball mills, pelletized, or spread over electrolyte membranes, and finally calcined at high temperatures to yield anodes for solid-oxide fuel cells (SOFCs).[11] The MON materials obtained in such bottom-up approaches, however, often suffer from poor transport performances that lead to increased power loss of the fuel cells and/or batteries. Each of the phases of the MON is composed of a closed heterointerface between the different phases that terminates the flow of currents to increase the inherent impedance.

Recently, a new class of MONs has been materialized through a different approach than the conventional assembly of nano-scale building blocks.[12–14] It was demonstrated that MONs having extended nanotextures can spontaneously emerge out of precursor alloys that consist of highly oxyphilic metals, such as early d-metals and lanthanides.[15–17] When subjected to an atmosphere containing oxygen (O_2), such precursor alloys are dissociated into metal and oxides as a result of the oxyphilic metal species being selectively converted into oxides. The infusion of oxygen atoms from the surface into the bulk of the precursor alloy develops a phase-connected MON comprising a nanometre-thick, interconnected network of metal and oxide (*i.e.*, nanophase separation).[16] The interconnected metal–oxide network in the MON leads to superior transport performances due to the spatially connected pathways of metal and oxide phases for electronic and ionic transport, respectively.[18–20] The phase-connected MON materials are, despite the inherent priority of spatial connectedness of material phases, still precluded from wide use in batteries or fuel cells due to the lack of a guiding principle to tune their phase texture toward maximized performances.

Herein, we report that a hybrid approach consisting of microscopic observations and mathematical simulations allows an understanding and even predictions of the mode of phase textures of MONs. *In situ* transmission electron microscopy (*in situ* TEM) has demonstrated that a layer-by-layer, nanometre-thick (2 through 10 nm) lamella texture of platinum (Pt) and cerium oxide (CeO_2) spontaneously emerges out of a precursor alloy of Pt_5Ce when

This journal is © the Owner Societies 2024

Phys. Chem. Chem. Phys., 2024, **26**, 14103–14107 | **14103**

subjected to an atmosphere consisting of O_2 and carbon monoxide (CO) at temperatures higher than 500 °C. The lower the O_2 fraction concerning the CO concentration, the more sluggish the texture formation and the more folded the phase texture that ranges from lamellae to mazes. Mathematical simulations based on a linearized reaction–diffusion model have shown that either a maze or lamella pattern tends to emerge when the atomic diffusivity of one of the metal species is in the order of 1/50 or 4/50 compared to that of the counterpart metal species, respectively. This simulation result supports a picture that the atomic diffusion of Ce, which is much more sluggish compared to that of Pt across the oxidating Pt_5Ce alloy, plays a predominant role in the emergence of Pt–CeO_2 MON. This work opens up a route towards a tuned phase texture of MONs by controlling the atomic diffusions of the constituent elements of the precursor alloys through temperature, alloy composition, and/or the composition of the oxidative atmosphere.

2. Experimental section

Pt_5Ce alloy was obtained by melting ingots of Pt and Ce metals at a mole ratio of Pt : Ce = 5 : 1 using an arc-torch in an argon atmosphere to avoid oxidation. The alloy ingot was crushed with a mortar and sieved to collect particles with an average diameter of 50 μm. The Pt_5Ce powder was then cut with a field-ion bombardment (FIB) apparatus down to a thickness of 80 nm. *In situ* TEM observation was performed on the thinly cut sample of Pt_5Ce using JEM-1000K RS TEM (JEOL) at Nagoya University, which was equipped with a specially designed atmosphere-controllable cell. The sample was exposed to a reactant gas consisting of CO and/or O_2 at 200 Pa, while the sample temperature was set at 500 °C throughout the experiments.

A turing proposed a mathematical model that mutual reactions between two diffusing components can lead to spatially uneven patterns (*i.e.*, the reaction–diffusion (RD) model).[21,22] The RD model has been extensively applied to different systems including patterns on the skin of animals, the embryotic emergence of organs, and non-biological systems such as nanophase separation of high-tensile alloys.[23–25] The RD model is generally described as a set of non-linear, time-dependent differential equations of two chemical species u and v:

$$\frac{\partial u}{\partial t} = f_u(u, v) + D_u \Delta u$$
$$\frac{\partial v}{\partial t} = f_v(u, v) + D_v \Delta v \tag{1}$$

This set of equations can be simplified in the form of a set of linear equations within a rational boundary condition to describe the pattern formation of nanophase-separated alloy systems as follows:

$$\begin{pmatrix} \dfrac{\partial u}{\partial t} \\ \dfrac{\partial v}{\partial t} \end{pmatrix} = \begin{pmatrix} a_u & b_u \\ a_v & b_v \end{pmatrix} \begin{pmatrix} u \\ v \end{pmatrix} + \begin{pmatrix} D_u & o \\ o & D_v \end{pmatrix} \begin{pmatrix} \Delta u \\ \Delta v \end{pmatrix} + \begin{pmatrix} c_u \\ c_v \end{pmatrix} \tag{2}$$

where each of the parameters a_u, b_u, a_v, and b_v is regarded as a constant in the vicinity of the origin of the (u, v) plane. See ESI† for the derivative of the linearized equation.

Numerical simulations were performed in cubic simulation boxes of 100 × 100 grids using a homemade software that was coded with C. The process of visualization of the simulation images from the mathematical model is described in detail in ESI,† Fig. S1. An array of complex variables was executed to generate different 2-dimensional patterns. A periodic boundary condition was applied to the whole of the simulating area. Both u and v were assumed to depend on time (t) and coordinates (r), and monotonously depend on the concentrations of the chemical species. The coefficients of a_v, and b_u in eqn (2) denote a reaction of the two metal species comprising the precursor alloy: Pt and Ce atoms, respectively.

3. Experimental results

In situ TEM has demonstrated that the Pt_5Ce precursor alloy is separated into different phases when subjected to an oxidative atmosphere, leading to the formation of intricate patterns consisting of different nanophases of Pt metal and cerium oxide (CeO_2) (see Videos S2(i) and S2(ii) in the ESI†). Ce metal in Pt_5Ce is oxidized to develop a CeO_2 phase due to its high oxygen affinity, driving the formation of intricate patterns consisting of Pt metal and CeO_2 phases. This phenomenon was only observed at temperature 500 °C and higher, and no phase separation was observed at a temperature lower than 500 °C due to the lack of energy to initiate oxidation. See Video S2(iii) in the ESI.†

A set of experiments was conducted to investigate the nanophase separation of the Pt_5Ce alloy, one in a gas mixture of CO and O_2 at partial pressures of 200 Pa and 100 Pa, and the other at partial pressures of 0 Pa and 200 Pa. As can be seen from the snapshots of *in situ* TEM in Fig. 1(a.2), a lamella pattern emerged when the Pt_5Ce alloy was exposed to a pure O_2 atmosphere. Continuous supply of O_2 further promoted the nanophase separation, which that led to a spatially ordered lamella pattern at an emergence rate of 20 nm s^{-1} (Fig. 1(a.3)). In the gas mixture of CO and O_2, an entangled, maze-like pattern emerged instead of the lamella pattern (Fig. 1(b.2)). CO here acts as an inhibitor and constrains the oxidation rate by intercepting some of the O species on the surface.[20] By increasing the CO concentration atmosphere, more O species were intercepted, which results in a more sluggish, maze-like pattern. Note that the emergence rate of the maze pattern was much lower than that of the lamella pattern: an aliquot of 120 s was necessary to accomplish the pattern formation, whereas the lamella pattern required only 5 s (Fig. 1(a.2) and (b.2)). We observed the same trend in simulations where a longer iteration time was required to generate a maze pattern compared to a lamella pattern (ESI,† Fig. S3).

$$\begin{pmatrix} a_u & b_u \\ a_v & b_v \end{pmatrix} = \begin{pmatrix} - & - \\ + & + \end{pmatrix} \tag{3}$$

Computational simulations were conducted on variable values of the off-diagonal terms of (a_u, a_v) and the diffusion

14104 | *Phys. Chem. Chem. Phys.*, 2024, **26**, 14103–14107
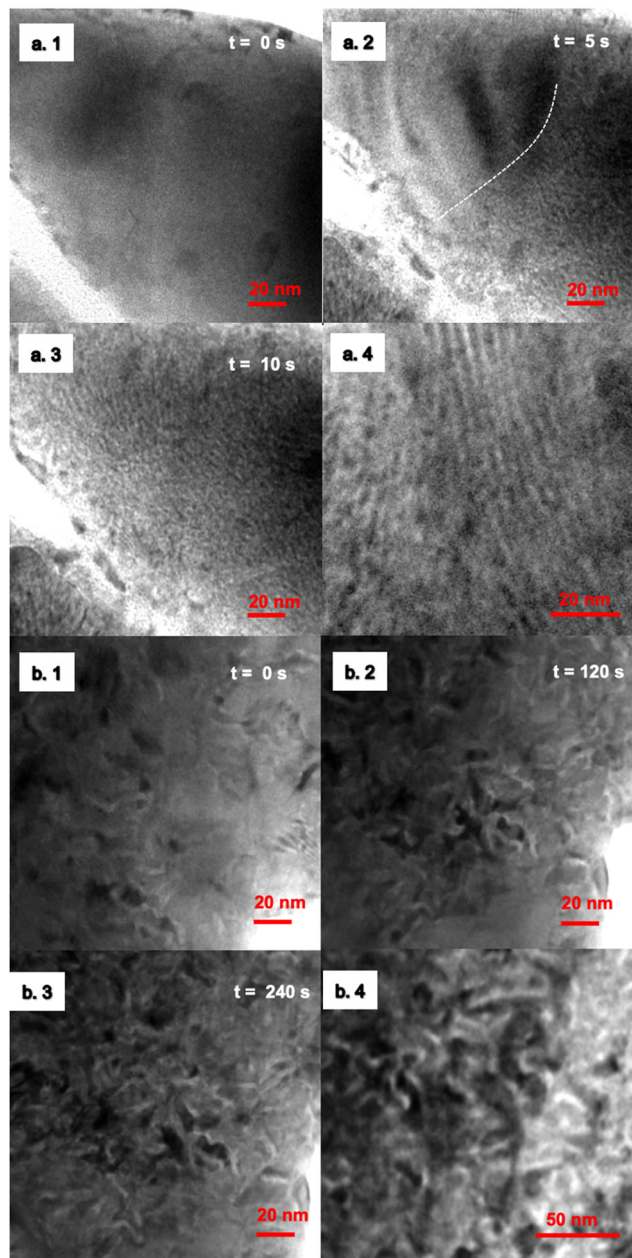
This journal is © the Owner Societies 2024

Fig. 1 Snapshots of *in situ* TEM images where lamellae and maze patterns were observed after Pt₅Ce alloy was subjected to an (a) O₂ and (b) CO : O₂; 2 : 1 environment. Wavefront of phase separation propagation indicated with a white broken line. Close view of the pattern formed as shown in (a.4) and (b.4) showing lamellae and maze, respectively.

coefficients of (D_u, D_v), setting the other parameters constant (ESI,† Fig. S4 and S5). First, we have noticed that the off-diagonal terms in the equation determine the nature of the "reaction" between the chemical species. When both a_v and b_u are the same in sign, the concentrations of the chemical species monotonously either diverge or converge with increasing time, being accompanied by no pattern formation. Only in the event that the off-diagonal terms are different in sign (eqn (3)), spatially uneven patterns can spontaneously emerge out of a uniform medium due to a competition between the diffusions of mutually reacting chemical species.
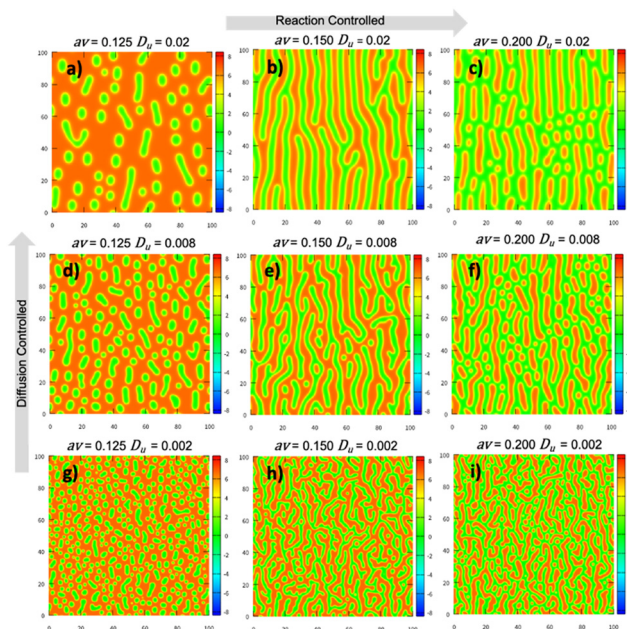

Fig. 2 Patterns obtained from simulation by triggering the reaction and diffusion terms. The a_v value was set to (0.125, 0.15 and 0.2) and the D_u value was set to (0.002, 0.008, 0.02). All the other parameters were set to constant.

We further computed the patterning evolution by considering the different parameters at the same time (Fig. 2). Fig. 2a corresponds to $a_v = 0.125$ and $D_u = 0.02$. With increasing a_v from 0.125 while fixing D_u, the pattern evolves from isolated spots to a lamella pattern that consists of a parallel array of stripes at $a_v = 0.150$ (Fig. 2b). The warm-colored region diminishes with the increase in a_v (Fig. 2c). As seen on the first column of Fig. 2 that corresponds to $a_v = 0.125$, the spotty phase becomes more highly distributed with the decrease in D_u (Fig. 2a, d and g). Another trend is recognized in the second column of Fig. 2 that corresponds to $a_v = 0.15$. The lamella pattern (Fig. 2b) is folded (Fig. 2e) with a decrease in D_u to develop a maze pattern when $D_u = 0.002$ (Fig. 2h). A similar trend is recognized for the third column of Fig. 2 that corresponds to $a_v = 0.20$, where the parallel array of broken stripes (Fig. 2c) is folded with decreasing D_u values (Fig. 2f) to finally reach a maze pattern (Fig. 2i).

The results of computational simulation demonstrate that spatially connected patterns are generated in a limited range of a_v and D_u, where D_u (0.02 to 0.002) is always 10 times or smaller than D_v (0.5). It is acknowledged that Ce atoms diffuse much more slowly than Pt atoms across a given Pt-rich alloy matrix.[26] We assign D_u and D_v to the diffusion constants of Ce and Pt, and accordingly, the variables of u and v to the local concentrations of Ce and Pt, respectively. The driving force of the nanophase separation of the Pt–Ce alloy precursor is most likely the exothermic oxidation of Ce, which leads to positive feedback of the Ce concentration (u) to both the Ce and Pt concentrations (v) through the positive parameters of a_u and a_v, respectively. Note that the feedback from the Pt concentration to the Ce and Pt concentrations is negligibly small ($b_v = 0.0$) or if

This journal is © the Owner Societies 2024

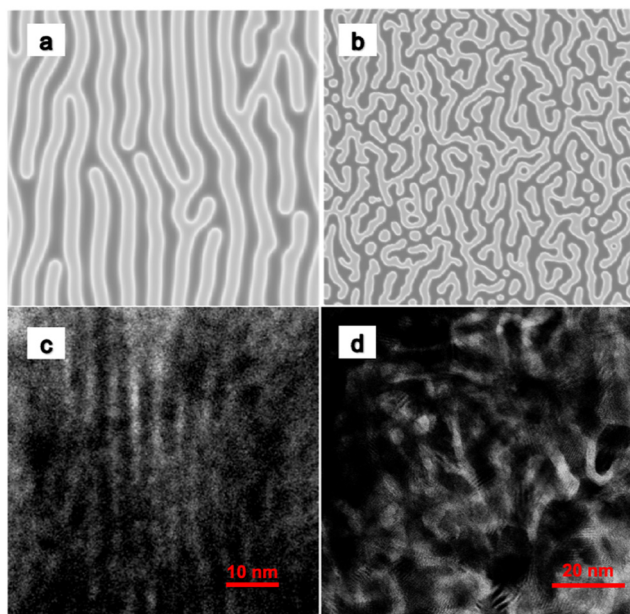*Phys. Chem. Chem. Phys.*, 2024, **26**, 14103–14107 | **14105**

Fig. 3 Simulation images (a) and (b) showing stripes and maze patterns, which were comparable to the experimental *in situ* TEM. $D_u = 0.02$ and $D_u = 0.002$ and snapshot images of *in situ* TEM taken under different conditions: (c) in pure O_2 and (d) in a $CO–O_2$ atmosphere.

anything, negative ($b_u = −0.05$), showing that Pt plays the role of an inhibitor for the nanophase separation of the Pt–Ce alloy precursor. Indeed, an increased Pt concentration can lower the concentration of the activator for the phase separation, namely, Ce. The diffusion of the fast-diffusing inhibitor, Pt, determines the distance between the two adjacent Pt phases that are separated by the activator, *i.e.*, the Ce phase.

Fig. 3 shows a similarity between the simulated patterns and the *in situ* TEM images. The computational simulation has demonstrated that either a lamella or maze pattern is generated when the diffusivity ratio for the different chemical species is $D_u/D_v = 0.02/0.50 = 1/25$ (Fig. 2b) or $0.002/0.50 = 1/250$ (Fig. 2h). Note that the lamella and maze patterns emerged in the atmosphere of pure O_2 gas and a mixture gas of $CO–O_2$, respectively. See ESI,† Fig. S6 for the scanning transmission electron microscope (STEM) image of the lamella pattern formed over a micrometre-sized area. The Ce oxidation not only drives the nanophase separation but can also lead to a rise in the local temperature of the precursor alloy at the propagation front of the Pt–CeO$_2$ MON. Considering the reducing nature of CO, it is rational to presume that the rise in the local temperature at the propagating front can be mitigated in the $CO–O_2$ atmosphere, leading to slow atomic diffusions. This presumption is supported by the experimental fact that the emergence rate of the maze pattern, 3 nm s^{-1}, was much slower than that of the stripe pattern, 20 nm s^{-1} (Fig. 1(b.3) and (a.3)). The diffusivity ratio steeply increases with lowering the temperature according to a widely acknowledged formula:

$$D_u/D_v \propto \exp\left(-\frac{(E_u − E_v)}{T}\right),$$

where E_u, E_v, and T correspond to the activation energy for the diffusions of Ce, Pt, and temperature, respectively ($E_u − E_v > 0$). We interpret the dramatic change in the mode of nanophase separation from the lamella to maze patterns as a result of the increased diffusivity ratio, which is further attributed to the mitigated Ce oxidation in the $CO–O_2$ atmosphere.

4. Conclusions

Through a hybrid approach of computational simulations and *in situ* transmission electron observations, we have successfully shed light to the emergence of metal–oxide nanocomposites (MONs) from precursor alloys *via* nanophase separation. The *in situ* TEM observation has allowed us to not only monitor the emergence of a MON but also quantify the emergence rate of the MON with different phase textures. The simulation has shown that the phase texture of the MON, such as a lamella or maze pattern, is predominantly determined by the ratio of the atomic diffusivity of the constituent atoms of the precursor alloy. The computational-experimental hybrid approach reported in this work has opened up a route to tailor the MON material by controlling the diffusivity of the constituent atoms of precursor alloys possibly through tuned temperature, alloy compositions, and/or atmospheres that promote nanophase separation of precursor alloys.

Author contributions

All authors contributed equally to the study concept and experimental design.

Conflicts of interest

The authors declare no conflict of interest.

Acknowledgements

References

1 S. Jeon, J. Seo, J. Shin, S. Lee, H. Seo, S. Lee, N. Tsvetkov, J. Kim, J. An and W. Jung, *Chem. Eng. J.*, 2023, **455**, 140611.

2 M. Li, J. Hou, Y. Fan, X. Xi, X. Fu and J. Luo, *Electrochim. Acta*, 2022, **426**, 140771.

3 Z. K. Ghouri, N. A. M. Barakat, H. Y. Kim, M. Park, K. A. Khalil, M. H. El-Newehy and S. S. Al-Deyab, *Arabian J. Chem.*, 2016, **9**, 219–228.

14106 | *Phys. Chem. Chem. Phys.*, 2024, **26**, 14103–14107

This journal is © the Owner Societies 2024

4 H. Alanazi., M. AlHaddad. and A. Shawky., *Mater. Res. Bull.*, 2023, **164**, 112248.

5 I. Yakovlev, S. Tikhov, E. Gerasimov, T. Kardash, K. Valeev, A. Salanov, Y. Chesalov, O. Lapina, O. Lomovskii and D. Dudina, *Materials*, 2023, **16**, 1074.

6 P. Mendes, Y. Song, W. Ma, T. Gani, K. Lim, S. Kawi and S. Kozlov, *Adv. Phys.: X*, 2023, **1**(1), 2175623.

7 Z. Wang, S. Xu, Q. Sui, J. Wang, B. Liu, H. Wen, T. Xiao, Q. Yuan, F. Zhao and J. Liu, *Rare Met.*, 2023, **42**(7), 2419–2432.

8 Z. Sun, J. Zhou and Q. Zhang, *Prog. Nat. Sci.: Mater. Int.*, 2021, **31**, 152–158.

9 J. Chen, J. Davies, A. S. Goodfellow, S. M. D. Hall, H. G. Lancaster, X. Liu, C. J. Rhodes and W. Zhou, *Prog. Nat. Sci.: Mater. Int.*, 2021, **31**, 141–151.

10 Y. B. Ma, Y. W. Wang, D. Zhang, X. Jia, Y. Wang, S. Zhou, T. Wagberg and G. Hu, *Rare Met.*, 2023, **42**(11), 3622–3629.

11 A. Hanifi, M. Laguna-Bercero, N. Sandhu, T. Etsell and P. Sarkar, *Sci. Rep.*, 2016, **6**, 27359.

12 P. Sutter, S. Tenney, F. Ivars-Barcelo, L. Wu, Y. Zhu and E. Sutter, *Nanoscale Horiz.*, 2016, **1**, 212–219.

13 T. K. Kim, K. J. Lee, J. Y. Cheon, J. H. Lee, S. H. Joo and H. R. Moon, *J. Am. Chem. Soc.*, 2013, **135**(24), 8940–8946.

14 M. Hadden, D. Martinez-Martin, K. Yong and Y. Ramaswamy, *Materials*, 2022, **15**, 2111.

15 T. Sakpal and L. Lefferts, *J. Catal.*, 2018, **367**, 171–180.

16 A. Strijevskaya, A. Yamaguchi, S. Shoji, S. Ueda, A. Hashimoto, Y. Wen, A. C. Wardhana, J. E. Lee, M. Liu, H. Abe and M. Miyauchi, *ACS Appl. Mater. Interfaces*, 2023, **15**(19), 23299–23305.

17 H. Nishiguchi, A. S. B. M. Najib, X. Peng, Y. Cho, A. Hashimoto, S. Ueda, T. Fujita, M. Miyauchi and H. Abe, *Adv. Sustainable Syst.*, 2020, **4**, 200041.

18 A. S. B. M. Najib, X. Peng, A. Hashimoto, S. Shoji, T. Lida, Y. Bai and H. Abe, *Chem. – Asian J.*, 2019, **14**, 2802–2805.

19 S. Shoji, A. S. B. M. Najib, M. Yu, K. Chen, H. Abe and M. Miyauchi, *Chem. Catal.*, 2022, **2**, 321–329.

20 Y. Wen, A. Hashimoto, A. S. B. M. Najib, A. Hirata and H. Abe, *Appl. Phys. Lett.*, 2021, **118**, 054102.

21 A. Turing, *Philos. Trans. R. Soc., B*, 1952, **237**, 37–72.

22 L. Menou, C. Luo and D. Zwicker, *J. R. Soc., Interface*, 2023, **20**, 20230244.

23 S. Kondo, M. Watanabe and S. Miyazawa, *Philos. Trans. R. Soc., A*, 2021, **379**, 20200274.

24 I. Heemskerk, *Dev. Biol.*, 2020, **460**, 86–98.

25 Y. Wen, H. Abe, K. Mitsuishi and A. Hashimoto, *Nanoscale*, 2021, **13**, 18987–18995.

26 P. Malacrida, M. Escudero-Escribano, A. Verdaguer-Casadevall, E. L. Stephens and I. Chorkendorff, *J. Mater. Chem. A*, 2014, **2**, 4234.

This journal is © the Owner Societies 2024

Phys. Chem. Chem. Phys., 2024, **26**, 14103–14107 | **14107**